Wiley Online Library
Early View publication on www.wileyonlinelibrary.com
(issue and page numbers not yet assigned;
citable using Digital Object Identifier – DOI)

Phys. Status Solidi A, 1–6 (2014) / DOI 10.1002/pssa.201431393

physica status solidi a
www.pss-a.com
applications and materials science

Multiple-layered nonwoven nanosheets consisting of multiwalled carbon nanotubes

Heon Ham[*,1], Eun-Hye Koo[2], Sang-Yong Ju[2], No-Hyung Park[3], Yong Jung Kwon[4], Hong Yeon Cho[4], Han Gil Na[4], Kwang Bo Shim[4], Won-Jae Lee[5], and Hyoun Woo Kim[,4]**

[1] Department of Liberal Arts and Sciences, and Nanomaterial Research Center, H&H Co. Ltd., Korea National University of Transportation, 50 Daehak-ro, Chungju-Si, Chungbuk 330-702, Korea
[2] Department of Chemistry, Yonsei University, Seoul 120-749, Korea
[3] Department of Textile Convergence of Biotechnology and Nanotechnology, Korea Institute of Industrial Technology, 1271-18 Sa 3-dong, Sangnok-gu, Ansan-Si, Gyeonggi-Do 426-910, Korea
[4] Department of Materials Science and Engineering, Hanyang University, 222 Wangsimni-ro, Seongdong-Gu, Seoul 133-791, Korea
[5] Department of Electronic Engineering, Gachon University, Seongnam 461-701, Korea

Received 29 May 2014, revised 5 September 2014, accepted 24 September 2014
Published online 16 October 2014

Keywords carbon nanotubes, graphitization, nanostructures, Raman spectroscopy, scanning electron microscopy, transmission electron microscopy

[*] Corresponding author: e-mail hh1001@hanyang.ac.kr, Phone: +82 16 9799 1901, Fax: +82 2 2220 2294
[**] e-mail hyounwoo@hanyang.ac.kr, Phone: +82 10 8428 0883, Fax: +82 2 2220 2294

We fabricated multiple-layered nonwoven multiwalled carbon nanotubes (MWCNT) sheets by means of treating MWCNTs with a spark plasma sintering process. We characterized the samples by Raman spectroscopy, X-ray diffraction (XRD), scanning electron microscopy, transmission electron microscopy, and the field effect mobility method. Each thin nonwoven MWCNT layer is mainly comprised of interlocked, intertwined, or interconnected MWCNTs. XRD and Raman spectra coincidentally revealed that the graphitization occurred in the course of transformation from pristine to nonwoven MWCNTs. The multiple-layered nonwoven MWCNTs showed a higher electrical conductance than a single-layered nonwoven MWCNTs sheet.

1 Introduction Nonwovens are highly engineered solutions made up of a variety of materials including fibers, powders, particles, adhesives, films and other materials that provide a multitude of functionalities, for instances, hygienic applications [1], interlinings [2], geotextiles [3, 4], carpet backings [5], automotive parts [6], filters [7, 8], and wipes [9], etc.

Nonwoven fabrics, which correspond to sheet or web structures bonded together by entangling filaments or fibers, are one of the oldest and simplest textile fabrics. Nonwoven fabrics were utilized mainly in protective clothing [10, 11]. However, in recent years, a nonwoven industry has grown abruptly and now started to find its application in other various industries. Nonwoven fabrics can be directly obtained from fibers, whereas traditional fabrics are prepared by the complicated procedures. Accordingly, a nonwoven material can save fabrication costs.

In the carbon industry, various carbon/carbon composites, including solid carbon fibers [12, 13], polyacrylonitrile-derived carbon fibers in a pyrolytic matrix [14], polylactic acid/MWVNT composites [15], and silicon-coated carbon nanotubes (CNTs) [16], have been used for fabrication of nonwoven structures.

The CNTs have excellent mechanical properties, including extraordinary flexibility, high strength, fracture toughness, and good resilience [17, 18]. In addition, the CNTs have good electrical and thermal properties [19, 20]. Accordingly, CNTs have been studied for their usage for fabricating nonwoven materials [15, 21]. Although it is possible that nonwovens made up of CNTs with larger diameters have lower tensile strength and poor cohesiveness, due to the decrease of van der Waals force between CNTs, it can be improved to some extent not only through functionalization of CNTs but also by the addition of

polymers [22]. The CNT-based nonwovens have been reported to have potential applications to a variety of devices, including field emission displays [23, 24], electromechanical actuators [25], supercapacitors [26], reinforced composite materials, and filters.

Up to the present, CNTs have been used for fabricating a variety of nonwoven materials. Single-walled CNT (SWCNT) nonwoven sheets were fabricated via floating chemical vapor deposition (CVD) [14]. The SWCNT buckypapers were prepared by the filtration of SWNT suspensions [27, 28]. Single-layered and aligned MWCNT nonwoven sheets were synthesized by low-pressure CVD [29–31]. Mixed buckypapers of SWCNTs/MWCNTs were synthesized by the filtration of the dispersed solution [32, 33].

In this study, for the first time, multiple-layered MWCNT nonwoven sheets were fabricated by treating MWCNTs with a spark plasma sintering (SPS) process. This process consistently produces a high-density compact in an extremely short sintering time. The high sintering rate can be attained due to internal heating of the sample, which maximizes the heating rate. In the short time of the SPS process, which does not allow the coarsening or grain growth, nanostructured materials with excellent mechanical properties can be easily fabricated. Accordingly, the agglomeration of the nonwoven nanosheets will be avoided. This SPS is a simple and low-cost process, and consumes less energy. We observe that the fabricated multilayered MWCNT nonwoven sheet is composed of many thin MWCNT nonwoven layers, each of which is made up of intertwined, interlocked or interconnected MWCNTs. MWCNTs have been selected as one-dimensional carbon sources in order to fabricate a multiple-layered MWCNT nonwoven sheet. To examine the electrical properties of nonwoven MWCNT, which is expected to be enhanced due to the multiple connections of MWCNTs, we have measured the current (I)–voltage (V) curves of single-/multilayered nonwoven MWCNT by means of the simple two probe method.

2 Experimental An Fe–Mo/MgO catalyst for synthesis of MWCNTs has been prepared as follows: $Fe(NO_3)_2{\cdot}6H_2O$ (purity: 99%, Aldrich), Mo solution (Aldrich, ICP/DCP standard solution) and MgO powder were mixed with alcohol and the resultant mixture was stirred for 1 h, ultimately Fe and Mo being embedded onto the MgO. The mixture was then filtered, with the residue being baked at 150 °C for 10 h in a vacuum ambient. The baked residue was ground into powder.

Hundred milligrams of Fe–Mo/MgO catalyst powder was placed in a quartz boat and then the quartz boat was inserted in the center of a quartz tube with an internal diameter of 20 mm and a length of 500 mm. The quartz tube was then mounted in an electrical tube furnace and heated to 700 °C in an Ar atmosphere. Subsequently, a gas mixture of Ar and CH_4 was kept flowing into the quartz tube at atmospheric pressure. The temperature was set to 700 °C for 30 min. The flow rates of CH_4 and Ar were 200 and 500 sccm, respectively.

In order to remove unwanted metallic or carbon materials, initial MWCNTs, which were not purified, first underwent a nitric acid refluxing process. Subsequently, oxidation of the acid-treated MWCNTs was carried out in air at 450 °C for 30 min, leaving behind MWCNTs that lost 20% of their initial weight. The MWCNTs were then heated at 1500 °C for 6 h at 1.3×10^{-5} Torr in a vacuum chamber to remove encapsulated metal catalysts. By means of this process, the purity of MWCNT was raised up to 98 wt.%.

The conversion of pristine MWCNTs to nonwoven MWCNTs was carried out in a vacuum chamber (at 10^{-5} Torr) using a Dr. sinter® model SPS-2080 PCS system (Sumitomo Coal mining Co., Japan). Two grams of MWCNTs were placed between two graphite punches in a cylindrical graphite (ISO-63) die. The MWCNTs were heated for 30 min at a heating rate of 100 °C min^{-1} at a pressure of 100 MPa until it reached 1800 °C. The applied direct current was in the range of 1500–2500 A (voltage <5 V) and the pulse duration and interval were 12 and 2 ms, respectively. As revealed in our previous paper [34], the pulse current flows through the MWCNTs during the SPS process, generating heat and thus providing energy to the MWCNTs.

In order to prepare a suspension, samples were dispersed in chlorobenzene by a bath sonicator for 15 min. The suspension was drop cast on a 100-nm thick SiO_2/Si substrate and the resultant particles on the substrate were observed with a scanning electron microscope (SEM; FEI-Nova Nano SEM 200 with a field emission gun) and a transmission electron microscope (TEM; JEOL-4010 microscope operating at 400 keV). X-ray powder diffraction (XRD) patterns were acquired with a Rigaku D/Max 2550 diffractometer using CuKα radiation ($\lambda = 1.5418$ Å).

Raman signals were obtained in a backscattering geometry using a home-built setup, which consists of a Jobin-Yvon Horiba triax 320 spectrometer (focal length: 320 mm, 1800 gratings/mm, resolution: 2 cm^{-1}) and a Si array CCD (Sympony, CCD-1024 × 256-BIDD-STE, 1024 × 256, 26 μm/pixel). In order to calibrate the Raman spectrometer, radiation with a wavelength of 546.073 nm emitted from a Hg lamp was used. A diode-pumped solid-state laser (wavelength of 532 nm) was used as an excitation source. The 100 objective lens (MPlanFL N, numerical aperture = 0.90, Olympus) was used to focus and make a diffraction-limited spot. Raman spectra were measured using 1.5 mW beam power and the total acquisition time was set in the range of 100–300 s. A suspension of MWCNT was drop casted on a 300-nm thick SiO_2/silicon wafer before measuring the Raman spectra. In the Raman spectra, laser power (<2 mW) was kept below the damage threshold (ca. 4 mW) of graphene to avoid any laser damage to samples.

In order to examine the electrical conductivity of the samples in terms of the field effect mobility method with a 4-probe technique, we measured the I–V curves by means of a source meter (Keithley Model 2400, OH, USA). The pristine and nonwoven MWCNTs were put on a silicon wafer with a size of 10×10 cm^2. We fabricated the Pt patterned device; the distance between two Pt electrodes is

3 μm, and the width of each electrode is 3 μm. All samples exhibit a linear *I*–*V* relation ranging from –1.0 to 1.0 V.

3 Results and discussion Figure 1a shows an image of a typical MWCNT sheet fabricated in this experiment. Figure 1b shows flat pieces exfoliated from the fabricated MWCNT sheet. The fabricated MWCNT sheet was broken into pieces in order to examine its cross section. Examination of the cross section revealed that the seemingly simple MWCNT sheet of Fig. 1a consisted of many thin layers shown in Fig. 1c and d. This is why the fabricated MWCNT sheet can be exfoliated.

Figure 2a and b shows SEM images of thin layers, consisting of the MWCNT sheet. We observe that the thin layers are MWCNT-based nonwoven materials, in which individual MWCNTs are clearly distinguished. Figure 2c and d shows the associated low-magnification and lattice-resolved TEM images, respectively, clearly exhibiting the intertwinned, interlocked or interconnected MWCNTs. All the above examinations suggest that the seemingly simple MWCNT sheet is made up of many thin MWCNT nonwoven layers, thus being able to be called multiple-layered MWCNT nonwoven sheets.

Figure 3a shows a low-magnification SEM image, indicating that carbon droplets were formed on the thin MWCNT nonwoven layers. Closer examination of the layers reveals that the carbon droplets with their diameter being tens of nanometers, have been formed on the surface of MWCNTs, as shown in Fig. 3b. Figure 3c shows a TEM image, revealing the existence of the unzipped MWCNT. Figure 3d shows a TEM image of a thin MWCNT nonwoven layer, which contains a partly graphitized area. Figure 3e is an enlarged image of the circled region of Fig. 3d, whereas Fig. 3f corresponds to an enlarged one of the circled region of Fig. 3e. Figure 3g is an associated SAED pattern, exhibiting a graphitic nature. Figure 3h shows a TEM image of a nonwoven layer, exhibiting the presence of graphene as well as MWCNTs. During the SPS process, a high current flows through the MWCNTs and a lot of heat will be generated. The heat will not only break the carbon bonds of the MWCNTs but also evaporate carbon atoms from the MWCNTs. The MWCNTs will be unzipped, interconnected

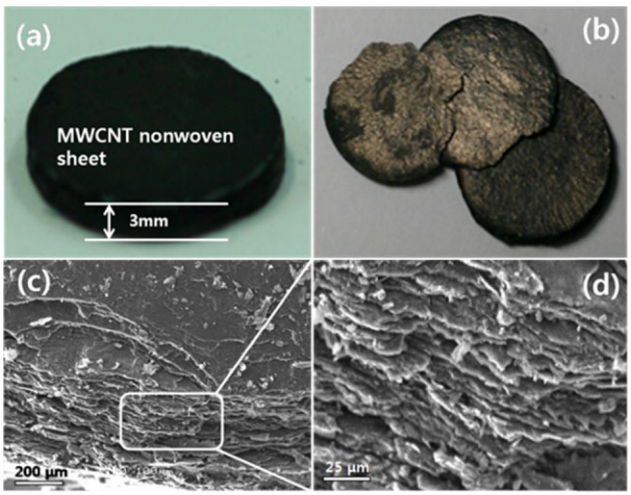

Figure 1 (a) Photograph of as-fabricated MWCNT nonwoven sheets, which are disc-shaped. (b) Photograph of flat pieces, which were exfoliated or separated from the fabricated MWCNT sheet. (c) Cross-sectional optical microscopy (OM) image of the MWCNT sheet, showing many thin layers. (d) Magnified OM image of the rectangular region in (c), which clearly shows many thin layers being overlapped.

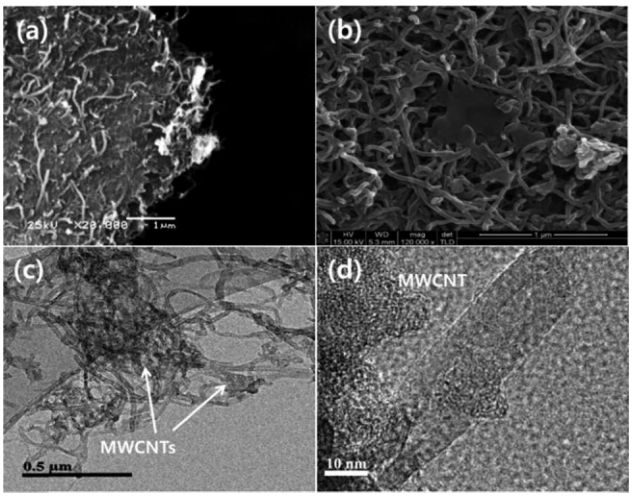

Figure 2 (a) Top-view SEM image of one of the many thin layers from the fabricated MWCNT nonwoven sheet. (b) Enlarged SEM image of a selected area in (a). (c) Low-magnification TEM image of MWCNTs. (d) Lattice-resolved TEM image of MWCNTs.

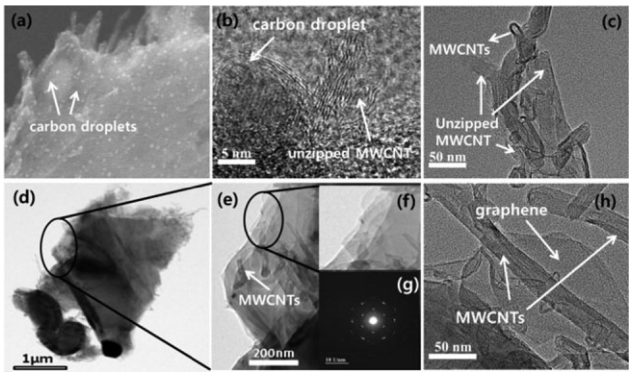

Figure 3 (a) Low-magnification SEM image, showing carbon droplets on a thin MWCNT nonwoven layer. (b) Lattice-resolved TEM image enlarging a carbon droplet in (a), which resides on MWCNTs in a thin MWCNT nonwoven layer. (c) TEM image of an unzipped MWCNT in a thin MWCNT nonwoven layer. (d) TEM image of a thin MWCNT nonwoven layer that contains a partly graphitized area. (e) An enlarged image of the selected circled area of figure (d). (f) An enlarged image of the selected circled area of figure (e). (g) SAED pattern of the circled area in (e). (h) TEM image of graphene in a thin MWCNT nonwoven layer.

with one another or converted into graphene or graphite. We surmise that evaporated carbon atoms will form carbon droplets on the surface of MWCNTs as the temperature drops after the SPS process.

Figure 4a shows a TEM image of a nonwoven MWCNT sheet. Figure 4b is an enlarged image of the squared region in Fig. 4a, clearly exhibiting the lattice plane images of MWCNTs. Figure 4c and d shows the enlarged images of the areas, which are designated as "A" and "B" in Fig. 4b, respectively, exhibiting turbostratic structures with regard to the wall of the MWCNTs. Figure 4e shows a SAED pattern with the characteristic of turbostratic MWCNT. During the SPS process, the high electric current and heat will cause the walls of MWCNTs to slip out of alignment, generating a turbostratic structure.

The fabricated nonwoven MWCNT sheet was further investigated by XRD and its XRD spectrum was compared with those of MWCNTs and graphite. As shown in Fig. 5, characteristic peaks of (002) reflection are found in all the spectra, because they have the same honeycomb lattice structure. As the material changes from pristine MWCNTs to nonwoven MWCNT sheets, the amount of one-dimensional (1D) tubular MWCNTs and two-dimensional (2D) graphene or graphite decreases and increases, respectively, and thus the (002) diffraction peak becomes sharper.

Figure 6a shows a Raman spectrum of the pristine MWCNTs, prior to the SPS process. The Raman spectrum of MWCNTs exhibits the D and concomitant D′ bands near 1350 and 1615 cm^{-1}, respectively, and also shows a large G peak near 1582 cm^{-1} and a 2D peak at 2695 cm^{-1}. Accordingly, the intensity ratio of D to G bands (I_D/I_G) is about 0.72. By comparing Fig. 6b with Fig. 6a, the I_D/I_G of

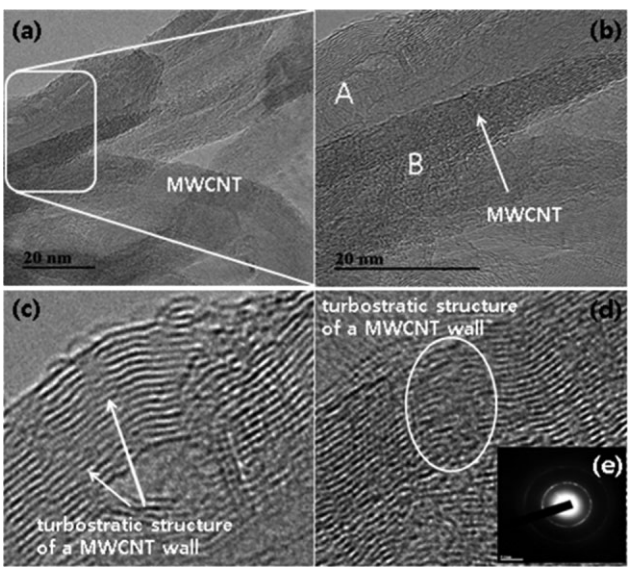

Figure 4 (a) TEM image showing MWCNTs in the MWCNT nonwoven sheet. (b) TEM image of the selected square area in (a). (c, d) Lattice-resolved TEM images of the area (c) "A" and (d) "B" in (b), exhibiting a turbostratic structure. (e) SAED pattern of the circled area in (d).

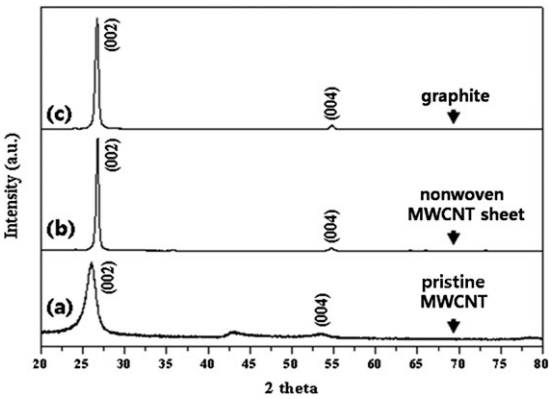

Figure 5 XRD spectra of (a) pristine MWCNT, (b) nonwoven MWCNT sheet, and (c) graphite.

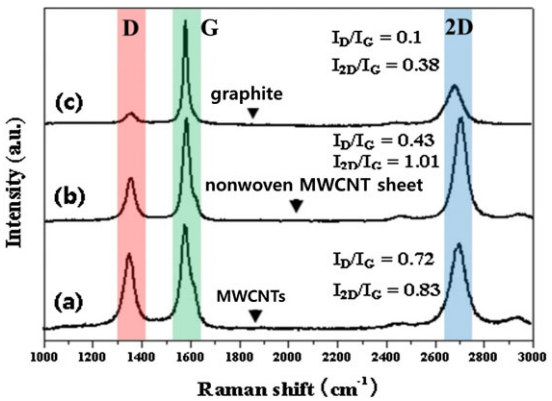

Figure 6 Raman spectra of (a) pristine MWCNT, (b) nonwoven MWCNT sheet, and (c) graphite. The spectra were offset to aid visualization. The excitation wavelength was 532 nm.

nonwoven MWCNT sheet (i.e., $I_D/I_G = 0.43$) is significantly lower than that of MWCNTs (i.e., $I_D/I_G = 0.72$). In other words, the fabricated nonwoven MWCNT sheet has a lower D peak intensity than the MWCNTs. This is because the fabricated nonwoven MWCNT sheet has fewer defects than the MWCNTs. Additionally, the intensity of 2D band (or G′) of the nonwoven MWCNT sheet is comparable to that of the G band (i.e., the intensity ratio between 2D and the G band (I_{2D}/I_G) is 1.01), presumably because a significant number of MWCNTs were unzipped or converted into graphene when the nonwoven MWCNT sheet was formed from MWCNTs by the SPS process. Since the SPS process will occur under high temperature and high electrical energy, it is possible that a lot of defects will be generated. Also, the process occurs in a closed environment and carbon atoms can be evaporated and saturated inside the chamber. When the temperature becomes lowered at the end of the SPS process, the evaporated carbon atoms may combine with defects on MWCNTs, decreasing the defect density.

Figure 7(a)–(c) shows the *I–V* curves of pristine MWCNT, a single-layered nonwoven MWCNT sheet, and

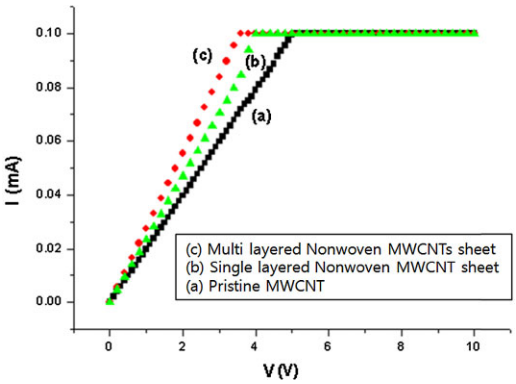

Figure 7 *I–V* curves of (a) pristine MWCNT, (b) single-layered nonwoven MWCNT sheet, and (c) multilayered nonwoven MWCNT sheet.

a multilayered nonwoven MWCNT sheet, respectively. All samples exhibit a linear *I–V* relation within the experimental conditions (from 0 to 10 V). Herein, since we have set the maximum current value, the current value above the maximum value cannot be recorded. The conductances of pristine MWCNT, single-layered nonwoven MWCNT sheet, and multilayered nonwoven MWCNT sheet were estimated to be 2.0×10^{-5}, 2.5×10^{-5}, and 2.8×10^{-5} S, respectively. Accordingly, the conductance of a single-layered nonwoven MWCNT sheet is 25% higher than that of pristine MWCNT. Furthermore, the conductance of multilayered nonwoven MWCNT sheet sheet is 40% higher than that of pristine MWCNT. Also, when we measure the *I–V* curve, we have used the samples with a fixed amount (i.e., dimension and weight) of products. Accordingly, the *I–V* behavior shown in Fig. 7 will not change upon the change of the *Y*-axis from current to current density.

Although the pristine MWCNTs have excellent electrical properties, nonwoven MWCNTs indicate an even higher electrical conductivity than the MWCNT sheet, because of the formation/connection of the MWCNTs. In the course of transformation to nonwoven sheets, the connection of MWCNTs has been created by a high DC pulse and high temperature. The local connection of nonwoven structures leads to the increase of the *I–V* slope, in comparison to that of MWCNTs. Furthermore, the *I–V* slope of multilayered nonwoven MWCNTs is a little higher than that of a single-layered one, presumably due to the increase of local connections. This result reveals that transformation of pristine to nonwoven MWCNT structure is favorable for enhancing the electrical conductivity.

4 Conclusions A multiple-layered nonwoven MWCNT sheet has been, for the first time, fabricated using MWCNTs and a SPS process. Each layer of the multiple-layered nonwoven MWCNT sheet is comprised of intertwined, interlocked or interconnected MWCNTs, which additionally contain carbon droplets, graphitic structures, and graphene. Moreover, turbostratic MWCNTs have been found in the as-fabricated multiple-layered nonwoven MWCNT sheet. XRD spectra confirm that the relative amounts of 1D MWCNTs and 2D graphene (or graphite) decreases and increases, respectively, by changing from pristine to nonwoven MWCNTs. The Raman spectra reveal that the value of I_D/I_G of nonwoven sheet (0.43) is higher and lower than that of graphite (0.1) and pristine MWCNT (0.72), respectively. The *I–V* slope of nonwoven nanosheets is higher than that of the pristine MWCNTs. Furthermore, the *I–V* slope of multilayered nonwoven MWCNTs is higher than that of single layered ones. This tendency results from the increase of local connections. This result reveals that transformation of pristine MWCNTs to nonwovens is an advantageous way to enhance its conductivity.

Acknowledgements This work was supported by a National Research Foundation of Korea (NRF) grant funded by the Korean government (MEST) (No. NRF-2013R1A2A2A01068438).

References

[1] K. Yeo, B. Hong, and H. Byun, J. Ind. Eng. Chem. **11**, 732 (2005).
[2] J. T. Fan and Y. N. Ng, Text. Res. J. **71**, 661 (2001).
[3] E. M. Palmeira, J. Tatto, and G. L. S. Araujo, Geotext. Geomembranes **31**, 1 (2012).
[4] A. Rawal, A. Kochhar, and A. Gupta, Geotext. Geomembranes **29**, 596 (2011).
[5] Y. Z. Shoshani, Text. Res. J. **60**, 452 (1990).
[6] D. V. Parikh, Y. Chen, and L. Sun, Text. Res. J. **76**, 813 (2006).
[7] H. Misslitz, K. Kreger, and H. W. Schmidt, Small **9**, 2053 (2013).
[8] R. Khajavi, M. M. S. Bahadoran, A. Bahador, and A. Khosravi, J. Ind. Text. **42**, 219 (2013).
[9] P. D. Dubrovski and M. Brezocnik, Fiber Polym. **13**, 363 (2012).
[10] B. G. Oakland, R. B. Dodd, D. J. Schabacker, and L. X. Clegg, Bull. Environ. Contam. Toxicol. **49**, 51 (1992).
[11] R. Jair and M. Raheel, Bull. Environ. Contam. Toxicol. **71**, 437 (2003).
[12] V. K. Varentsov, V. I. Varentsova, and I. A. Bataev, Russ. J. Appl. Chem. **85**, 1220 (2012).
[13] W. Cantwell, P. Curtis, and J. Morton, Composites **14**, 301 (1983).
[14] L. R. Bradley, C. R. Bowen, B. McEnaney, and D. C. Johnson, Carbon **45**, 2178 (2007).
[15] I. Krucinska, B. Surma, M. Chrzanowski, E. Skrzetuska, and M. Puchalski, Text. Res. J. **83**, 859 (2013).
[16] K. Evanoff, J. Benson, M. Schauer, I. Kovalenko, D. Lashmore, W. J. Ready, and G. Yushin, ACS Nano **6**, 9837 (2012).
[17] J. P. Salvetat, J. M. Bonard, N. H. Thompson, A. J. Kulik, L. Forro, W. Benoit, and L. Zuppiroli, Appl. Phys. A **69**, 255 (1999).
[18] S. H. Lee, H. Kim, S. Hang, and S. K. Cheong, Compos. Sci. Technol. **73**, 1 (2012).
[19] Y. Inoue, Y. Suzuki, Y. Minami, J. Muramatsu, Y. Shimamura, K. Suzuki, A. Ghemes, M. Okada, S. Sakakibara, H. Mimura, and K. Naito, Carbon **49**, 2437 (2011).
[20] J. Hone, M. C. Liaguno, N. M. Nemes, A. T. Johnson, J. E. Fischer, D. A. Walters, M. J. Casavant, J. Schmidt, and R. E. Smalley, Appl. Phys. Lett. **77**, 666 (2000).
[21] L. Song, L. Ci, L. Lv, Z. Zhou, X. Yan, D. Liu, H. Yuan, Y. Gao, J. Wang, L. Liu, X. Zhao, Z. Zhang, X. Dou,

W. Zhou, G. Wang, C. Wang, and S. Xie, Adv. Mater. **16**, 1529 (2004).
[22] J. N. Coleman, W. J. Blau, A. B. Dalton, E. Munoz, S. Collins, B. G. Kim, J. Razal, M. Selvidge, G. Vieiro, and R. H. Baughman, Appl. Phys. Lett. **82**, 1682 (2003).
[23] J. M. Bonard, N. Weiss, H. Kind, T. Stöckli, L. Forró, K. Kern, and A. Châtelain, Adv. Mater. **13**, 184 (2001).
[24] S. Fan, M. G. Chapline, N. R. Frankin, T. W. Tombler, A. M. Cassell, and H. Dai, Science **283**, 512 (1999).
[25] R. H. Baughman, C. Cui, A. A. Zakhidov, Z. Iqval, J. N. Barisci, G. M. Spinks, G. G. Wallace, A. Mazzoldi, D. D. Rossi, A. G. Rinzler, O. Jaschinski, S. Roth, and M. Kertesz, Science **284**, 1340 (1999).
[26] A. B. Dalton, S. Collins, E. Munoz, J. M. Razal, V. H. Ebron, J. P. Ferraris, J. N. Coleman, B. G. Kim, and R. H. Baughman, Nature **423**, 703 (2003).
[27] S. Wang, Z. Liang, G. Pham, Y.-B. Park, B. Wang, C. Zhagn, L. Kramer, and P. Funchess, Nanotechnology **18**, 095708 (2007).
[28] J. G. Park, J. Smithyman, C.-Y. Lin, A. Cooke, A. W. Kismarahardja, S. Li, R. Liang, J. S. Brooks, C. Zhang, and B. Wang, J. Appl. Phys. **106**, 104310 (2009).
[29] Z. Yang, T. Chen, R. He, G. Guan, H. Li, L. Qiu, and H. Peng, Adv. Mater. **23**, 5436 (2011).
[30] F. Hao, Z. Wang, P. Luo, J. Lou, J. Li, J. Wang, S. Fan, K. Jiang, and H. Lin, J. Mater. Chem. **22**, 22756 (2012).
[31] J.-H. Pöhls, M. B. Johnson, M. A. White, R. Malik, B. Ruff, C. Jayasinghe, M. J. Schulz, and V. Shanov, Carbon **50**, 4175 (2012).
[32] J. G. Park, S. Li, R. Laing, X. Fan, C. Zhang, and B. Wang, Nanotechnology **19**, 185710 (2008).
[33] J. G. Park, J. Louis, Q. Cheng, J. Bao, J. Smithyman, R. Liang, B. Wang, C. Zhang, J. S. Brooks, L. Kramer, P. Fanchasis, and D. Dorough, Nanotechnology **20**, 415702 (2009).
[34] H. Ham, N. H. Park, I. Kang, H. W. Kim, and K. B. Shim, Chem. Commun. **48**, 6672 (2012).

